SCIENTIFIC REP♀RTS

OPEN

Critical heat flux enhancement in pool boiling through increased rewetting on nanopillar array surfaces

Thien-Binh Nguyen[1], Dongdong Liu[1], Md Imrul Kayes[2], Baomin Wang[2], Nabeel Rashin[1], Paul W. Leu[2] & Tuan Tran (ID)[1]

Boiling is a key heat transfer process for a variety of power generation and thermal management technologies. We show that nanopillar arrays fabricated on a substrate enhance both the critical heat flux (CHF) and the critical temperature at CHF of the substrate and thus, effectively increase the limit of boiling before the boiling crisis is triggered. We reveal that the enhancement in both the CHF and the critical temperature results from an intensified rewetting process which increases with the height of nanopillars. We develop a predictive model based on experimental measurements of rewetting velocity to predict the enhancement in CHF and critical temperature of the nanopillar substrates. This model is critical for understanding how to control boiling enhancement and designing various nanostructured surfaces into specific applications.

Boiling is a central phenomenon in technological and industrial applications as diverse as thermal management in electronics, power generation and chemical processing[1–3]. In such applications, it is of immense importance to enhance the energy efficiency by increasing the critical heat flux (CHF), the highest heat flux a boiling substrate can achieve, as well as reducing operational risks caused by the notorious "boiling crisis", a catastrophic failure in boilers or heat exchanging devices[4]. The boiling crisis occurs on a boiling substrate when excessive vaporisation of liquid forms a vapour layer that severely impedes heat transfer through the substrate. This leads to abrupt jump in surface temperature and subsequently irreversible damages to the substrate of the boiling equipment. The temperature T_c at which CHF occurs therefore is directly connected to the boiling crisis; a boiling system operating at temperature higher than T_c inevitably drifts towards the boiling crisis. As a result, an enhancement in boiling performance, without triggering the boiling crisis, requires significant increases in both the critical heat flux and critical temperature T_c.

A large body of research has been dedicated to understanding the mechanism of nucleate boiling, a boiling regime in which latent heat transfer is dominant compared to convective heat transfer. With increasing surface temperature, CHF is the upper bound of heat flux in the nucleate boiling regime before the boiling crisis occurs[5]. Various microscale models have been proposed to capture nucleate boiling heat transfer mechanisms[6]. In addition, numerous key parameters affecting the heat flux in the nucleate boiling regime have been identified, e.g., surface roughness ranging from nano- to micro-scales[7], and wettability[8]. Nonetheless, a robust mechanistic prediction of nucleate boiling heat transfer for a wide range of boiling conditions, including the surface properties, is still not available[9].

To increase the critical heat flux, numerous methods have been explored following two major approaches: fluid modification and surface treatment. The former approach, which uses additives[10,11] or nanoparticles[12], has not been widely applicable as it puts constraints on fluid selection and operating conditions of the boiling system[13]. The latter approach includes either treatments to enhance surface wettability[14,15], or surface morphological alteration with porous coatings[16,17], artificial fins[18–20] and nano/microstructures[13,21]. Although numerous surface modification methods have been found to increase CHF, in particular those utilising nano/microstructures, the

[1]School of Mechanical and Aerospace Engineering, Nanyang Technological University, 50 Nanyang Avenue, Singapore, 639798, Singapore. [2]Department of Industrial Engineering and Department of Mechanical Engineering and Materials Science, University of Pittsburgh, Pittsburgh, 15261, USA. Correspondence and requests for materials should be addressed to T.T. (email: ttran@ntu.edu.sg)
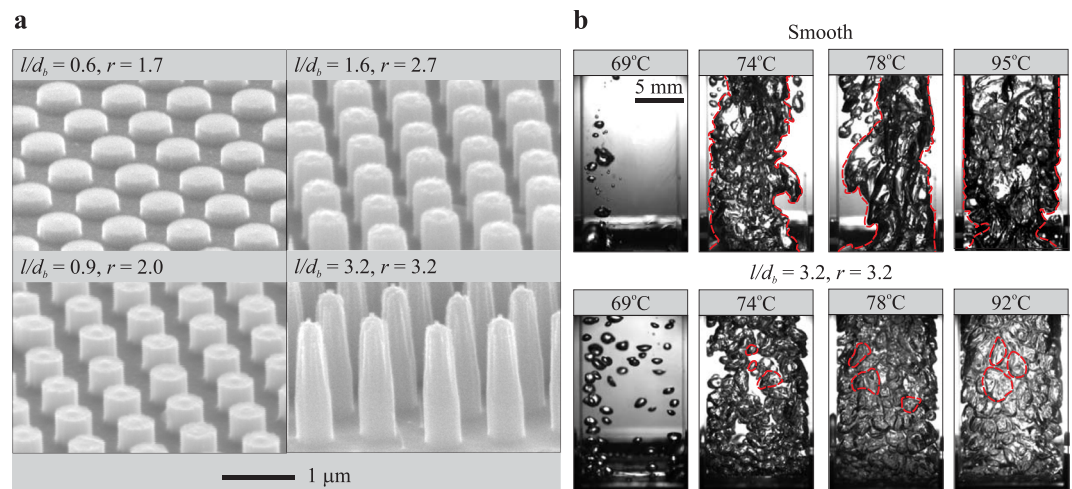
Figure 1. SEM images showing nanopillar substrates of different pillar dimensions: the ratio l/d_b, defined as the ratio between the pillar height l and base diameter d_b, and the corresponding surface roughness r are indicated in the labels. (**b**) Representative snapshots showing boiling phenomenon on the smooth substrate (top panel) and the nanopillar substrate having $r = 3.2$ (bottom panel) at several surface temperatures T. While the smooth surface produces vapour bubbles which have tendency to coalesce (e.g., at $T = 74\,°C$) and form vapour columns (e.g., at $T = 78\,°C$), the nanopillar substrate produce bubbles which have a narrow size distribution tend to evolve separately without merging. The vapour column and bubbles are highlighted by red dashed lines.

roles of surface structures at different length scales in changing the heat flux and the critical temperature remain elusive. On one hand, it was shown that the wickability effect is the major cause of enhancement in CHF[13,21], i.e., the CHF value was shown to increase linearly with the wicked volume flux for various substrate materials and different types of structures ranging from nanoscales to microscales[21]. On the other hand, the separate effect of variation in nanoscale structures on CHF and the critical temperature is still a standing question. Although it has been suggested that nanoscale structures may intensify the wetting velocity, which is a crucial factor leading to CHF enhancement[15,22], the relation between a systematic change in nanoscale structures, wetting velocity and CHF has not been established. Moreover, little effort has been made to relate surface wettability or nanoscale structures to the change in the critical temperature T_c.

In this study, we investigate the boiling phenomenon of FC-72 on nanostructured surfaces. Fluorinert liquid FC-72 is an ideal coolant liquid commonly used in various heat management applications owning to its low boiling point at 56 °C. We show that modifying the surface morphology at nanoscales leads to significant enhancement in the boiling performance, including both the critical heat flux and the critical temperature. By using nanopillars with systematically varying heights on silicon substrates, we demonstrate scalable boiling enhancement with increasing height of nanopillars. We propose and experimentally verify a mechanistic and predictive model relating the nanopillar-induced increase in rewetting to the enhancement in both CHF and critical temperature.

Results and Discussion

Enhancement in critical heat flux and nucleate boiling limit.
We systematically vary the height l of nanopillars fabricated on silicon substrates (Fig. 1a) and show that increasing l leads to enhancement in both the critical heat flux (CHF) and the upper limiting temperature of nucleating boiling. The nanopillars are fabricated by an inductively coupled plasma reactive ion etching (ICPRIE) process that directly modifies the surface without adding coating layers that may induce additional thermal resistance to the substrate[23]. Typically, the quantity used for characterising the upper limiting temperature is either the CHF temperature T_c, or the Leidenfrost temperature T_L. The nanopillars with the base diameter $d_b \approx 440$ nm are arranged in a hexagonal lattice with the lattice pitch $p \approx 800$ nm. The pillar height l is varied from 260 nm to 1390 nm. The differences in boiling behaviours and performances between these substrates therefore are attributed to variation in l, or alternatively the surface roughness $r = A_t/A_p$. Here A_t is the total surface area due to the presence of the nanopillars, and A_p is the projected boiling area. In our experiment, r ranges from 1 for the smooth silicon substrate to 3.2 for the nanopillar substrate with $l = 1390$ nm.

To qualitatively evaluate the effect of the nanopillars on boiling, we first compare the boiling behaviours between the smooth substrate and the nanopillar substrate with $r = 3.2$ at several surface temperatures T (Fig. 1b). Although the onset of boiling occurs at $T \approx 69\,°C$ for both substrates, the size of bubbles generated on the smooth substrate varies much more broadly than that on the nanopillar substrate. At higher temperature, the bubble dynamics on the two substrates become even more contrasting: while the bubbles on the smooth substrate tend to merge and create either large bubbles or vapour columns starting from the substrate, those generated on the nanopillar substrate have much lesser tendency to merge and appear more uniform in size. We note that it is not likely for bubbles to coalesce after their detachment from the substrate due to liquid inertia and surface tension, thus the coalescence process mainly occurs between consecutive bubbles generated from the same nucleation site before
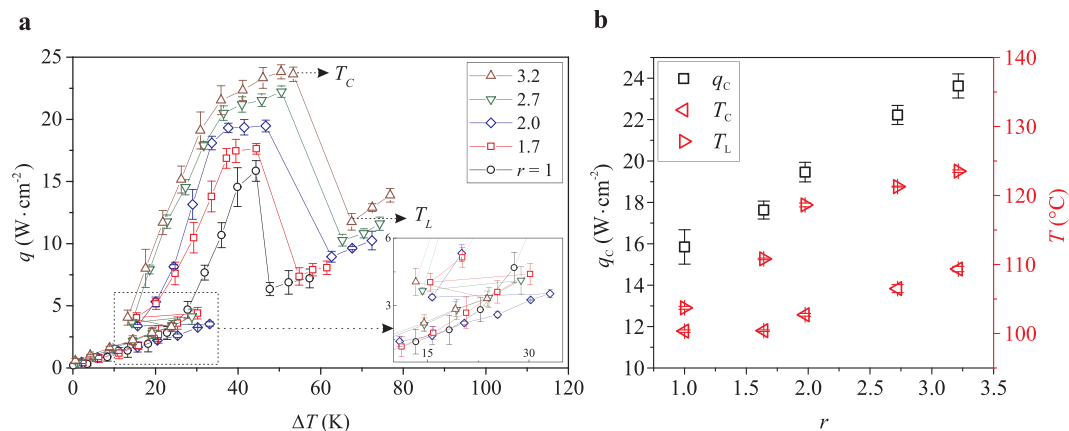
Figure 2. Heat flux q versus wall superheat ΔT for smooth substrate ($r = 1$) and nanopillar substrates. Error bars represent the standard deviation from multiple experiments. (**b**) Dependence of critical heat flux q_c (open squares), CHF temperature T_c (left-pointing triangles), and Leidenfrost temperature T_L (right-pointing triangles) on surface roughness r.

detachment. This strongly suggests that resistance to coalescence, as well as the uniform size of bubbles generated from the nanopillar substrate result from an effective rewetting process, which facilitates bubble detachment from the surface. We hypothesise that deviation in boiling behaviours of nanopillar substrates from the smooth one, therefore, originates from the nanopillar-induced enhancement in the rewetting process.

We now quantify the effect of nanopillars on the boiling performance by measuring the heat flux q for each substrate as a function of the superheat $\Delta T = T - T_b$, where $T_b = 56\,°C$ is the boiling temperature of FC-72 at atmospheric pressure. In Fig. 2a, we show the dependence of q on ΔT for the smooth and all the nanopillar substrates (See Supplementary Information for the uncertainty analysis of the heat flux and surface temperature measurements). Starting from $\Delta T = 0$, q first gradually increases due to natural convection until it reaches the onset of nucleate boiling ($\Delta T \approx 30$ K for all tested substrates). In this so-called natural convection regime, since the nanopillars are much smaller than the thermal boundary layer thickness, their presence causes negligible effect to the heat flux, which is dictated by the convective fluid flow outside of the thermal boundary layer. Here, the boundary layer thickness is roughly $57\,\mu m$, estimated using the ratio between the natural convection heat transfer coefficient and the thermal conductivity of FC-72[24].

As ΔT increases past the onset of nucleate boiling, the heat flux on nanopillar substrates, denoted as q^n, deviates substantially from that on the smooth substrate. In particular, q^n after the system transitions into the nucleate boiling regime is achieved at much lower superheat compared to that when system is still in the natural convection regime (inset of Fig. 2a). For instance, for the substrate with $r = 2$, $q = 3.3\,W\cdot cm^{-2}$ is achieved at $\Delta T \approx 16$ K when the system is in the nucleate boiling regime, whereas a slight increase in heat flux, $q \approx 3.5\,W\cdot cm^{-2}$, is achieved at much higher superheat $\Delta T \approx 33$ K in the natural convection regime. On the smooth substrate, however, the heat flux increases *smoothly* as the system transitions into the nucleate boiling regime. The presence of nanopillars causes a substantial jump in heat flux as soon as the system transitions to the nucleate boiling regime because the heat transfer mechanism is more efficient for the nanopillar substrates. The homogeneous spread of nucleation sites, high generation frequency and narrow size distribution of bubbles on nanopillar substrates (see Supplementary Information, Fig. S1) results in the sudden discontinuity in the boiling curve.

With the superheat increasing beyond the onset of nucleate boiling, bubbles are generated with higher frequency and larger size, intensifying forced convection in the bulk liquid and subsequently enhancing the heat flux q. For each substrate, q increases to the CHF q_c at the critical temperature T_c, beyond which it drops sharply due to excessive vapour generation and lack of replenishing liquid to the substrate. The heat flux reaches its minimum value at the so-called Leidenfrost temperature T_L, or the upper limit of nucleate boiling. The sudden drop in heat flux at T_L often triggers drastic spike in surface temperature causing the notorious "burn-out" in boiling applications. Thus, designing heat-dissipating substrates with high T_L is as practically important as enhancing the critical heat flux.

We observe considerable enhancement in both q_c and T_L on nanopillar substrates. In Fig. 2b, we show the dependences of q_c and T_L on the surface roughness r. Both q_c and T_L increase monotonically with increasing r (or equivalently with l). Compared to the smooth substrate ($r = 1$), q_c and T_L on the nanopillar substrate with $r = 3.2$ increase $\approx50\%$ and $\approx25\,°C$, respectively. The enhancement in both q_c and T_L is a remarkable feature of the nanopillar substrates as opposed to those fabricated with larger scale structures. It was observed that micro-structures only enhance the heat flux without increasing the Leidenfrost temperature; typically, T_L decreases with increasing height of microstructures[25]. Separate investigations on hierarchical substrates, i.e., microstructured surfaces covered with nano-grass, reported enhancement in *either* the Leidenfrost temperature[26–28], or the heat flux[13,27,29–34].

Mechanism of heat transfer enhancement on nanopillar substrates. To control the effects of nanopillars on enhancing q_c and T_L, we now investigate the heat transfer mechanism on nanopillar substrates. From qualitative observations of the differences in bubble generation between the nanopillar substrates and the smooth one, we postulate that the major contributing factor leading to the observed change in q_c and T_L
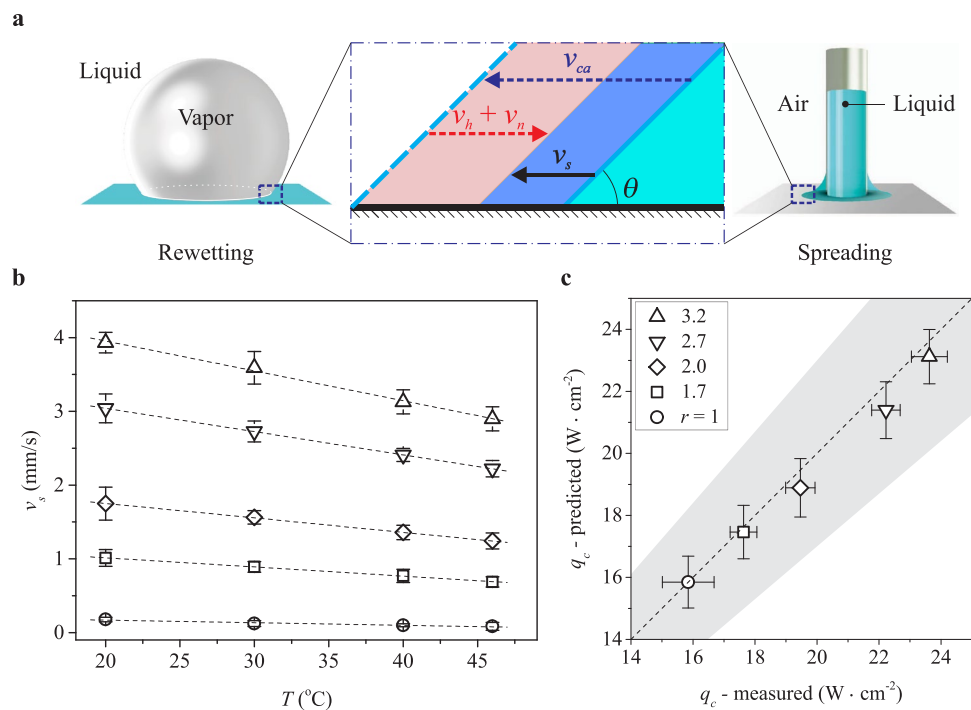
Figure 3. (**a**) Schematics showing similarities between the rewetting process in pool boiling (left panel) and the spreading process (right panel) from a capillary, in particular at the three-phase contact line (highlighted in the middle panel). (**b**) Apparent spreading velocity v_s of FC-72 on different substrates over a range of temperature from 20 °C to 46 °C. (**c**) Critical heat flux q_c predicted using Eqn. 2 versus the measured values for smooth substrate ($r = 1$) and nanopillar substrates. The uncertainty for the predicted heat flux comes from that of the spreading velocity measurements. The shaded area indicates a 15% deviation from the measured data.

is the nanopillar-induced rewetting process. We note that in the case of hierarchical structured surfaces, i.e., micro-structures covered by nano-grass, enhancement in q_c was observed, but due to a very different mechanism: the enhancement in volume of liquid wicking through the microstructures brings more liquid to the surface and subsequently leads to an increase in heat flux by latent heat of evaporation. The wicking process, however, is not possible for nanopillars due to the tremendous viscous stress induced in flows confined in such small length scales between pillars[13]. Thus, wicking is excluded as the cause of heat flux enhancement for our nanopillar substrates, which have interspacing between pillar $\approx$ 360 nm.

We focus on the advancing contact line of liquid to explore how the nanopillar-induced rewetting process leads to heat transfer enhancement. Taking advantage of the similarity between the rewetting process of vapour bubbles and the spreading process of liquid (illustrated in Fig. 3a), the dynamics of the advancing contact line can be studied separately in the case of spreading liquid on nanopillar substrates[15,22]. We note that the rewetting process has been the focus of numerous detailed studies[13], which revealed contributing factors such as surface-induced capillary force[13], hydrostatic and hydrodynamic forces[22], reshaping effects[35] and vaporisation[36]. For the nanopillar substrates, we determine the dominant effects and their contribution to the heat transfer by investigating the spreading of liquid from a capillary tip onto heated substrates (see Fig. 3a). By varying the surface temperature and tracking the three-phase contact-line (TCL) as the liquid spreads, we determine the temperature dependence of the apparent spreading velocity v_s on each nanopillar substrate.

The surface temperature can be varied from room temperature $T_r = 20$ °C up to 46 °C without causing the liquid to boil. Although the displacement of the TCL results from various coupled effects, we simplify the analysis by decomposing v_s into several independent components (Fig. 3b):

$$v_s = v_{ca} - v_n - v_h, \tag{1}$$

where the component v_{ca} is caused by capillary force on the substrate and therefore is a function of the surface roughness r only. The component v_h represents the reduction in spreading velocity as liquid absorbs heat from the surface and evaporates. Thus, if the substrate is not heated, i.e., $T = T_r$, it follows that $v_h = 0$ because there is no heat transferred from the surface to the liquid. The velocity component v_n represents the reduction in spreading velocity due to natural evaporation of liquid. In the case of liquid spreading in air, this component is nonzero and depends on the partial pressure of vapour, whereas in the case of boiling, it vanishes as bubbles generated during boiling of liquid are filled only with saturated vapour. Here, we have neglected contributions to TCL displacement from hydrostatic pressure of the liquid column, and from capillary pressure at the upper liquid surface in the tube due to the small gap between the capillary tube and the substrate.

We postulate that the increase in heat flux on nanopillar substrates results from nanopillar-induced enhancement in wetting. This is suggested from the linear correlation between the critical heat flux of different substrates and the spreading velocity v_s measured on respective substrates at surface temperature $T = 20\,°C$ (see Supplementary Information Fig. S2). In other words, the presence of nanopillars intensifies the rewetting process, leading to an added amount of liquid brought to and subsequently evaporated from the surface. Among the contributing components to the apparent spreading velocity, v_{ca} inherits the effect of r on capillary wetting, thus has a direct relation to the enhanced rewetting process. In addition, as the surface temperature for spreading liquid was set lower than the liquid's boiling temperature, we assume that with constant surface temperature, v_n remains fixed for all the substrates, i.e., $v_n^n = v_n^s$, where the superscripts n and s respectively indicate quantities of the nanopillar substrates and the smooth one. We recall that v_{ca} is independent of T and $v_h(T_r) = 0$. As a result, at room temperature T_r, the spreading velocity difference $\delta v_s(T_r) = v_s^n(T_r) - v_s^s(T_r)$ between a nanopillar substrate and the smooth one *only* depends on the change in capillary velocity between the two substrates $\delta v_{ca} = v_{ca}^n - v_{ca}^s$. Thus, δv_{ca} can be estimated as $\delta v_{ca} \approx \delta v_s(T_r)$.

We measure the spreading velocity v_s for all nanopillar substrates and the smooth substrate (see Fig. 3b). The spreading velocity increase $\delta v_s(T_r)$ is calculated for each nanopillar substrate to obtain δv_{ca}. The spreading velocity increases with increasing nanopillar height due to the increasing energetic favourability of wetted nanopillar surfaces of increasing height. The energy of the different dry nanopillar substrates is approximately the same. However, the energy of different wetted nanopillar substrates decreases with increasing height due to the larger interface between the liquid and solid nanopillar array. This energy difference drives the spreading of the FC-72, and thus, the spreading velocity increases with increasing nanopillar height. We note that for a nanopillar substrate with projected boiling area A_p, the increase in capillary velocity δv_{ca} leads to a mass increase of evaporated liquid $\rho_l A_d \delta v_{ca}$, where A_d is the time-averaged dry area during boiling on A_p. At CHF, A_d can be estimated using the classic boiling model by Zuber[37]: $A_d = KA_p$, with $K \approx 0.131$[4,37,38]. The enhancement in heat transfer at CHF, i.e., of a nanopillar substrate compared to the smooth substrate, can be calculated as $\delta Q_c = h_{fg}\rho_l A_d \delta v_{ca}$. As a result, we can estimate the heat flux at CHF, denoted as q_c^n, through each nanopillar substrate using that through the smooth one q_c^s and the heat flux enhancement $\delta Q_c/A_p = K\rho_l h_{fg} \delta v_{ca}$ as follows:

$$q_c^n = q_c^s + K\rho_l h_{fg} \delta v_{ca}. \tag{2}$$

We note that the heat flux at CHF on smooth substrates depends on the surface temperature and can be predicted using the classical model for nucleate boiling by Zuber[37]. A comparative study between the model and our boiling data on the smooth substrate shows an excellent agreement (see Methods for details). Thus Eqn. 2 provides a direct prediction of the heat flux through nanopillar substrates based on the enhancement in spreading velocity. In Fig. 3c, we show a comparison between the heat flux predicted using Eqn. 2 and one measured experimentally for all the substrates. The agreement between the predicted CHF and the measured values for all nanopillar substrates strengthen our hypothesis that the enhanced heat flux is caused by nanopillar-induced enhancement in rewetting. The results also suggest that the boiling crisis is mainly dictated by the intensity of the rewetting process, and the increase in critical heat flux is a direct consequence of the faster rewetting velocity using higher nanopillars.

Prediction of critical heat flux temperature on nanopillar substrates. We now explore how nanopillars-induced enhancement in rewetting affects the surface temperature T_c at CHF. Recall that the critical heat flux for nanopillar substrates can be predicted using that on the smooth substrate and the enhancement in rewetting velocity. We extend this argument to estimate T_c of nanopillar substrates. First, we determine the heat transfer coefficient h_{TCL} associated with liquid vaporisation at the three-phase contact line (TCL) by considering the volume Ω of liquid evaporated at TCL per unit time due to heat absorption from the nanopillar substrates. If we denote θ the contact angle of FC-72, Ω can be calculated as $\Omega = v_h A_d \tan\theta$ (see Fig. 3a for illustration). On one hand, the rate of latent heat required to evaporate Ω is $\rho_l \Omega h_{fg}$. On the other hand, the heat rate supplied from the substrate is $h_{TCL}(T - T_l)A_d$, where T_l is the liquid temperature. Balancing the rate of latent heat of evaporation and the heat rate supplied from the substrate gives the energy balance $\rho_l \Omega h_{fg} = h_{TCL}(T - T_l)A_d$. Thus, the heat transfer coefficient h_{TCL} can be obtained by taking derivative with respect to T of the energy balance, assuming that h_{TCL} is independent of T: $h_{TCL} = \rho_l h_{fg}\tan\theta dv_h/dT$. Taking into account the relation between the spreading velocity v_s and v_h (Eqn. 1) and recalling that v_{ca} is independent of T, we have $dv_h/dT = dv_s/dT$, thus arrive at the equation to determine h_{TCL} for each substrate:

$$h_{TCL} = \rho_l h_{fg} \tan\theta \frac{dv_s}{dT}. \tag{3}$$

The central argument of our analysis for nanopillar-induced enhancement in heat flux is that the heat transfer increase takes place at TCL where capillary wetting and evaporation are significantly altered by the presence of nanopillars. As shown in Fig. 4a, h_{TCL} calculated using Eqn. 3 increases linearly with the surface roughness, or equivalently, the height of nanopillars. This implies that the enhancement due to both conduction at the solid-liquid interface and convection on nanopillar substrates are secondary effects. The total heat transfer coefficient h^n on nanopillar substrates can then be estimated using the total heat transfer coefficient h^s on the smooth substrate and the enhancement in heat transfer coefficient at TCL:

$$h^n \approx h^s + K(h_{TCL}^n - h_{TCL}^s) + C = h^s + K\rho_l h_{fg} \tan\theta \frac{d(v_s^n - v_s^s)}{dT} + C, \tag{4}$$
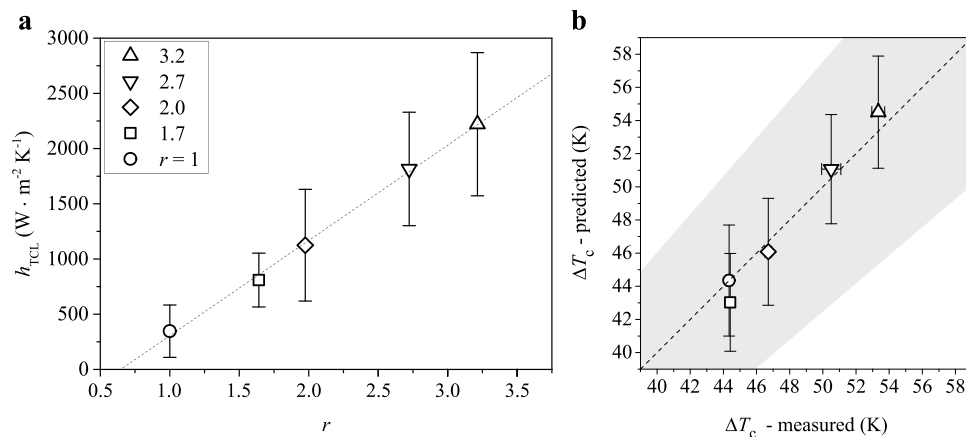
Figure 4. (**a**) Heat transfer coefficient at the three-phase contact line h_{TCL} versus surface roughness r. (**b**) Critical heat flux temperature T_c predicted using Eqn. 5 versus the measured values for substrates with different r. The shaded area indicates a 15% deviation from the measured data.

where the prefactor K is needed for the enhancement at TCL and the constant $C = 425\text{W} \cdot \text{m}^{-2} \cdot \text{K}^{-1}$ accounts for the additional heat transfer caused by the flow induced by displacement of bubbles from nanopillar substrates. Since there is no obvious difference in bubble dynamics between nanopillar substrates, we use a fixed constant C for all nanopillar substrates to represent the heat transfer increase due to displacement of bubbles. In deriving Eqn. 4, we also assume insignificant variation in h between the spreading and boiling processes for a fixed substrate. We note that Eqn. 4 can be applied at CHF due to the linear dependence of v_s on T (see Fig. 3b). The heat transfer coefficient at CHF on the smooth substrate can be determined using the heat transfer balance $q_c^s = h^s(T_c^s - T_b)$, which gives $h^s = q_c^s/(T_c^s - T_b)$. Here T_c^s is the wall temperature at CHF on the smooth substrate and T_b is the boiling temperature of the liquid. Similarly, we have $q_c^n = h^n(T_c^n - T_b)$, where T_c^n is the wall temperature at CHF on nanopillar substrates. Taking the predicted heat flux q_c^n and the heat transfer coefficient h^n on nanopillar substrates respectively from Eq. 2 and Eq. 4, T_c^n can be predicted as:

$$T_c^n - T_b = \frac{q_c^n}{h^n}. \tag{5}$$

In Fig. 4b, we compare the predicted superheat temperatures $\Delta T_c = T_c - T_b$ and the experimental ones at CHF for all substrates. Although the predicted values of ΔT_c carries the uncertainty of the spreading velocity measurement on nanopillar substrates, they fall within 15% deviation from the experimentally measured ones, highlighting a remarkable agreement between the predicted and experimental data.

Conclusions

In summary, we show that nanopillars fabricated on boiling substrates induce a substantial effect on the boiling behaviours in the nucleate boiling regime. In particular, increasing the height of nanopillars effectively leads to considerable enhancement in both heat flux and surface temperature at CHF. We attribute such enhancement to the nanopillar-induced increase in rewetting velocity, which can be measured in a separate wetting experiment. Based on the observations that the rewetting velocity increases for substrates with higher nanopillars, as well as the assumption that the enhancement in heat flux dominantly takes place at the three-phase contact line, we develop a mechanistic model to predict both the heat flux and the temperature at CHF of nanopillar substrates. Our model takes into account the nanoscales of the pillars, and thus, excludes the wicking motion, or imbibition of fluid, as plausible mechanisms for heat transfer enhancement. As a result, the enhanced capillary force due to the presence of nanopillars is the major cause of the intensified rewetting process and subsequent increases in heat flux and temperature at CHF.

The enhancement in both of these critical quantities in pool boiling is a remarkable feature of nanopillar substrates in comparison with nano/micro-engineered substrates in which only either one can be increased. By using only nanopillars with a systematic variation in height and well-defined geometrical dimensions, we have established a direct link between the enhancement in capillary force and the boiling performance of a substrate. This provides new insights about design of surface textures not only to amplify the heat flux, but also to achieve an enhancement in the temperature at CHF, an often less discussed but equally important quantity in preventing boiling crisis.

Methods

Fabrication of nanopillar substrates. The nanopillar silicon substrates are obtained by inductively coupled plasma reactive ion etching (ICPRIE). The fabrication process consists of three steps, (1) manufacture of the etching mask, (2) etching the underlying silicon by ICPRIE, and (3) removal of etching mask. Polystyrene (PS) nanospheres are utilised to generate the etching mask. First, a monolayer of nanospheres with the diameter of 800 nm are self-assembled in the air-water interface[39–41]. Subsequently the monolayer is transferred to a P-type
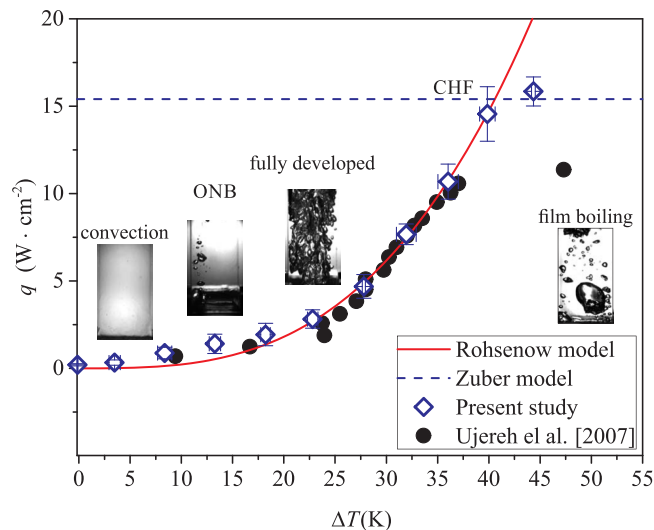
Figure 5. Comparison between the boiling curve measured on silicon smooth surface in the present study and the one obtained by Ujereh *et al.*[42]. The solid line represents the heat flux predicted by Rohsenow model, and the dashed line represent the critical heat flux predicted by Zuber model[37].

boron-doped (100) silicon substrate, which has been cleaned with acetone, methanol, isopropanol and then dried with nitrogen gas. After the substrate is dried in air at room temperature, reactive ion etching (RIE) with oxygen is applied to reduce the diameter of nanospheres to the required size ($\approx$440 nm).

After the etching mask is manufactured, ICPRIE is used to etch the silicon substrate to fabricate silicon nanopillars with desired dimensions. During the process, SF_6 and C_4F_8 with optimal ratio of 33:82 are supplied. These gases respectively serve as the etching gas and passivation gas. Different height nanopillars are obtained by varying the duration of this step. It should be noted that when the time duration is longer than 5 minutes the PS mask is impacted and the nanopillar base diameter is different from the etching mask. When the etching is completed, the PS mask is removed by ultrasonication in acetone for 5 minutes.

Boiling experiment. The experimental setup used to measure the heat flux through different substrates consists of three sections: heating, testing and condensation. In the heating section, a cartridge heater embedded in a cylindrical copper rod is used to generate heat. The copper rod is insulated from the surrounding environment by a Teflon holder. In the testing section, a boiling substrate, which is either smooth silicon wafer or a nanopillar substrate, is placed between the copper rod and a glass cuvette of lateral size 10 mm × 10 mm. The test substrate is cleaned by ethanol and acetone in a ultrasonic bath and rinsed with distilled water before each experiment. The cuvette is filled with degassed FC-72 as a working liquid. The cuvette is enclosed by a stainless-steel container; the gap between the cuvette and the container is circulated with hot water of temperature 55.5 ± 0.5 °C to keep the temperature of the working liquid close to boiling point. The container has two glass windows on two opposite sides allowing optical recording of the boiling phenomena. A condenser is placed on top of the container to collect vapour generated from the working liquid. The cooling power of the condenser is adjusted to keep the vapour pressure inside the cuvette at atmospheric pressure.

The vapour pressure is measured by pressure transducer (Gefran) and maintained at atmospheric pressure by adjusting the cooling power of a Peltier module. The temperature is measured by K-type thermocouples and the boiling process is recorded by a high-speed camera (SA-5, Photron). Three thermocouples are distributed along the asymmetrical axis of the copper cylinder. The temperatures measured by these thermocouples are used to calculate the heat flux q through the test substrate and the surface temperature T. The heat flux in the vertical direction is approximated with the assumption that the rate of heat loss to the side is constant[43,44]. Thus the heat flux through the substrate is estimated as:

$$q = 0.5 k_c (4T_2 - T_1 - 3T_3) \Delta x_c^{-1}. \tag{6}$$

where k_c is the thermal conductivity of copper, T_1, T_2, T_3 are obtained from the thermocouples in the copper rod, and $\Delta x_c = 7$ mm is the distance between the thermocouples. There are three layers between the top thermocouple and the top surface: a copper layer (7 mm), a thermal glue layer ($\approx$10 μm) and the silicon substrate (500 μm). The surface temperature T of the test substrate is then estimated by the one-dimensional heat conduction equation:

$$T = T_3 - q(\Delta x_c k_c^{-1} + \Delta x_g k_g^{-1} + \Delta x_s k_s^{-1}), \tag{7}$$

where $\Delta x_c / k_c$, $\Delta x_g / k_g$ and $\Delta x_s / k_s$ are the heat resistance of copper, thermal glue, and silicon substrate respectively. For each tested substrate, the heat flux q and the corresponding superheat $\Delta T = T - T_b$ are measured when the system is in the steady state and with temperature steps of 5 K. The experimental uncertainty is obtained by repeating the experiment three times.

Experimental Validation.　The measurement procedure and analysis are validated by comparing the heat transfer data obtained on the smooth substrate to the well-known dataset obtained by Ujereh *et al.*[42], as well as to classical model, including the one for nucleate boiling heat transfer by Rohsenow[45] and the one for critical heat flux by Zuber[37] (see Fig. 5). In particular, the critical heat flux on a smooth substrate is:

$$q_c^s = K\rho_v^{1/2}h_{fg}[g\sigma(\rho_l - \rho_v)]^{1/4},\qquad(8)$$

where $K \approx 0.131$ is an empirical parameter.

References

1. Dhir, V. Boiling heat transfer. *Annual review of fluid mechanics* **30**, 365–401 (1998).
2. Karwa, N., Gambaryan-Roisman, T., Stephan, P. & Tropea, C. A hydrodynamic model for subcooled liquid jet impingement at the leidenfrost condition. *International Journal of Thermal Sciences* **50**, 993–1000 (2011).
3. Xu, X. & Qian, T. Single-bubble dynamics in pool boiling of one-component fluids. *Physical Review E* **89**, 063002 (2014).
4. Carey, V. P. *Liquid-vapor phase-change phenomena* (CRC Press, 2007).
5. Theofanous, T., Tu, J., Dinh, A. & Dinh, T.-N. The boiling crisis phenomenon: Part i: nucleation and nucleate boiling heat transfer. *Experimental Thermal and Fluid Science* **26**, 775–792 (2002).
6. Kim, J. Review of nucleate pool boiling bubble heat transfer mechanisms. *International Journal of Multiphase Flow* **35**, 1067–1076 (2009).
7. Kim, D. E., Yu, D. I., Jerng, D. W., Kim, M. H. & Ahn, H. S. Review of boiling heat transfer enhancement on micro/nanostructured surfaces. *Experimental Thermal and Fluid Science* **66**, 173–196 (2015).
8. Betz, A. R. *et al.* Boiling heat transfer on superhydrophilic, superhydrophobic, and superbiphilic surfaces. *International Journal of Heat and Mass Transfer* **57**, 733–741 (2013).
9. Dhir, V. K. Mechanistic prediction of nucleate boiling heat transfer–achievable or a hopeless task? *Journal of Heat Transfer* **128**, 1–12 (2006).
10. Laurila, T., Carlson, A., Do-Quang, M., Ala-Nissila, T. & Amberg, G. Thermohydrodynamics of boiling in a van der waals fluid. *Physical Review E* **85**, 026320 (2012).
11. Liu, J., Do-Quang, M. & Amberg, G. Thermohydrodynamics of boiling in binary compressible fluids. *Physical Review E* **92**, 043017 (2015).
12. Kamatchi, R. & Venkatachalapathy, S. Parametric study of pool boiling heat transfer with nanofluids for the enhancement of critical heat flux: a review. *International Journal of Thermal Sciences* **87**, 228–240 (2015).
13. Dhillon, N. S., Buongiorno, J. & Varanasi, K. K. Critical heat flux maxima during boiling crisis on textured surfaces. *Nature communications* **6** (2015).
14. Zupančič, M., Steinbücher, M., Gregorčič, P. & Golobič, I. Enhanced pool-boiling heat transfer on laser-made hydrophobic/superhydrophilic polydimethylsiloxane-silica patterned surfaces. *Applied Thermal Engineering* **91**, 288–297 (2015).
15. Rahman, M. M., Pollack, J. & McCarthy, M. Increasing boiling heat transfer using low conductivity materials. *Scientific reports* **5** (2015).
16. Xu, P., Li, Q. & Xuan, Y. Enhanced boiling heat transfer on composite porous surface. *International Journal of Heat and Mass Transfer* **80**, 107–114 (2015).
17. Tang, B., Zhou, R., Lu, L. & Zhou, G. Augmented boiling heat transfer on a copper nanoporous surface and the stability of nano-porosity in a hydrothermal environment. *International Journal of Heat and Mass Transfer* **90**, 979–985 (2015).
18. Zhong, D., Meng, J., Li, Z. & Guo, Z. Experimental study of saturated pool boiling from downward facing surfaces with artificial cavities. *Experimental Thermal and Fluid Science* **68**, 442–451 (2015).
19. Zhong, D., Meng, J., Li, Z. & Guo, Z. Critical heat flux for downward-facing saturated pool boiling on pin fin surfaces. *International Journal of Heat and Mass Transfer* **87**, 201–211 (2015).
20. Li, C. H. & Rioux, R. P. Independent and collective roles of surface structures at different length scales on pool boiling heat transfer. *Scientific reports* **6** (2016).
21. Rahman, M. M., Olceroglu, E. & McCarthy, M. Role of wickability on the critical heat flux of structured superhydrophilic surfaces. *Langmuir* **30**, 11225–11234 (2014).
22. Kim, B. S., Choi, G., Shin, S., Gemming, T. & Cho, H. H. Nano-inspired fluidic interactivity for boiling heat transfer: impact and criteria. *Scientific reports* **6**, 34348 (2016).
23. Zupančič, M., Može, M., Gregorčič, P., Sitar, A. & Golobič, I. Evaluation of enhanced nucleate boiling performance through wall-temperature distributions on pdms-silica coated and non-coated laser textured stainless steel surfaces. *International Journal of Heat and Mass Transfer* **111**, 419–428 (2017).
24. Bejan, A. & Kraus, A. D. *Heat transfer handbook*, vol. 1 (John Wiley & Sons, 2003).
25. Nair, H. *et al.* The leidenfrost temperature increase for impacting droplets on carbon-nanofiber surfaces. *Soft matter* **10**, 2102–2109 (2014).
26. Kwon, H.-m, Bird, J. C. & Varanasi, K. K. Increasing leidenfrost point using micro-nano hierarchical surface structures. *Applied Physics Letters* **103**, 201601 (2013).
27. Ahn, H. S. *et al.* Pool boiling experiments on multiwalled carbon nanotube (mwcnt) forests. *Journal of Heat Transfer* **128**, 1335–1342 (2006).
28. Sathyamurthi, V., Ahn, H., Banerjee, D. & Lau, S. Subcooled pool boiling experiments on horizontal heaters coated with carbon nanotubes. *Journal of Heat Transfer* **131**, 071501 (2009).
29. Vemuri, S. & Kim, K. J. Pool boiling of saturated fc-72 on nano-porous surface. *International communications in heat and mass transfer* **32**, 27–31 (2005).
30. Wu, W. *et al.* Nucleate boiling heat transfer enhancement for water and fc-72 on titanium oxide and silicon oxide surfaces. *International Journal of Heat and Mass Transfer* **53**, 1773–1777 (2010).
31. Chen, R. *et al.* Nanowires for enhanced boiling heat transfer. *Nano letters* **9**, 548–553 (2009).
32. Launay, S., Fedorov, A., Joshi, Y., Cao, A. & Ajayan, P. Hybrid micro-nano structured thermal interfaces for pool boiling heat transfer enhancement. *Microelectronics Journal* **37**, 1158–1164 (2006).
33. Li, C. *et al.* Nanostructured copper interfaces for enhanced boiling. *small* **4**, 1084–1088 (2008).
34. Im, Y., Joshi, Y., Dietz, C. & Lee, S. S. Enhanced boiling of a dielectric liquid on copper nanowire surfaces. *Int. J. Micro-Nano Scale Transp* **1**, 79–95 (2010).
35. Cooper, M. & Chandratilleke, T. Growth of diffusion-controlled vapour bubbles at a wall in a known temperature gradient. *International Journal of Heat and Mass Transfer* **24**, 1475–1492 (1981).
36. Zou, A., Singh, D. P. & Maroo, S. C. Early evaporation of microlayer for boiling heat transfer enhancement. *Langmuir* **32**, 10808–10814 (2016).
37. Zuber, N. Hydrodynamic aspects of boiling heat transfer (thesis). Tech. Rep., California. Univ., Los Angeles; and Ramo-Wooldridge Corp., Los Angeles (1959).

38. Linehard, J. & Dhir, V. K. Extended hydrodynamic theory of the peak and minimum pool boiling heat fluxes. *Tech. Rep* (1973).
39. Ye, X. & Qi, L. Two-dimensionally patterned nanostructures based on monolayer colloidal crystals: controllable fabrication, assembly, and applications. *Nano Today* **6**, 608–631 (2011).
40. Yu, J. *et al.* Preparation of high-quality colloidal mask for nanosphere lithography by a combination of air/water interface self-assembly and solvent vapor annealing. *Langmuir* **28**, 12681–12689 (2012).
41. Moon, G. D. *et al.* Assembled monolayers of hydrophilic particles on water surfaces. *ACS Nano* **5**, 8600–8612 (2011).
42. Ujereh, S., Fisher, T. & Mudawar, I. Effects of carbon nanotube arrays on nucleate pool boiling. *International Journal of Heat and Mass Transfer* **50**, 4023–4038 (2007).
43. Cooke, D. & Kandlikar, S. G. Pool boiling heat transfer and bubble dynamics over plain and enhanced microchannels. *Journal of Heat Transfer* **133**, 052902 (2011).
44. Yao, Z., Lu, Y.-W. & Kandlikar, S. Effects of nanowire height on pool boiling performance of water on silicon chips. *International Journal of Thermal Sciences* **50**, 2084–2090 (2011).
45. Rohsenow, W. M. A method of correlating heat transfer data for surface boiling of liquids. Tech. Rep., Cambridge, Mass.: MIT Division of Industrial Cooporation (1951).

Acknowledgements

Author Contributions

T.T. and P.W.L. conceived the experiment, T.B.N., D.L., M.I.K., B.W., and N.R. conducted the experiment, T.B.N., D.L., and T.T. analysed the results. All authors reviewed the manuscript.

Additional Information

Supplementary information accompanies this paper at https://doi.org/10.1038/s41598-018-22693-z.

Competing Interests: The authors declare no competing interests.

Publisher's note: Springer Nature remains neutral with regard to jurisdictional claims in published maps and institutional affiliations.